Cold Crystallization of Narrow Molecular Weight Fractions of PEEK

C. Fougnies,[†] M. Dosière,*[,†] M. H. J. Koch,[‡] and J. Roovers[§]

Université de Mons-Hainaut, Laboratoire de Physicochimie des Polymères, Place du Parc, 20, B-7000 Mons, Belgium; European Molecular Biology Laboratory, Hamburg Outstation, EMBL c/o DESY, Notkestrasse, 85, D-22603 Hamburg, Germany; and Division of Chemistry, National Research Council of Canada, Ottawa, Ontario K1A OR9, Canada

Received June 9, 1999; Revised Manuscript Received September 13, 1999

ABSTRACT: Several amorphous narrow molecular weight fractions of poly(aryl ether ether ketone) or PEEK have been heated from below their glass transition temperature to above their final melting point. The semicrystalline morphology induced by cold crystallization and its thermal evolution are studied by time-resolved simultaneous small-angle X-ray scattering (SAXS), wide-angle X-ray diffraction, and differential scanning calorimetry. The long period and the crystalline and the amorphous thicknesses are computed from the correlation function of the SAXS curves. The evolution of the structural parameters of the various semicrystalline samples can be reconciled with the existence of a single distribution of lamellae which undergoes reorganization during the continuous heating. The reorganization process as well as the semicrystalline morphology depends on the molecular weight of the fractions. The amorphous thickness strongly increases with the molecular weight while the thermal evolution of the thickness of the crystalline layers is similar for all fractions. These experimental results support the view that the larger degree of entanglements of the high molecular weight samples impedes the reorganization mechanism with the consequence that the apparent melting temperature decreases with increasing average molecular weight.

Introduction

Poly(aryl ether ether ketone) (PEEK) is an aromatic polymer which exhibits a rather interesting combination of mechanical and chemical properties.[1] It can be used as a thermoplastic matrix in polymer composites where high-temperature resistance and high strength are required.[2,3] Beside its industrial applications, PEEK has received considerable interest in theoretical studies, and it is now admitted that PEEK as well as PET could be considered as model compounds for aromatic stiff-chain polymers. Though the crystallization behavior has been widely studied using various techniques including differential scanning calorimetry (DSC),[4−10] small-angle X-ray scattering (SAXS), and wide-angle X-ray diffraction (WAXD),[11−24] and electron (TEM)[25−29] and optical microscopies (OM),[30−33] some uncertainties still remain concerning the morphology of semicrystalline PEEK samples. In particular, the existence of two populations of lamellar crystals with a different crystalline thickness has been proposed to account for the double melting behavior of semicrystalline PEEK samples.[17,18,25] Since an insertion process of secondary lamellae within the primary grown crystals has been ruled out, it has been proposed that the secondary crystals grow in separate lamellar stacks (dual lamellar stack model).[34] This model, which is based on the assumption that the largest length computed from the correlation function corresponds to the crystal thickness L_c, also accounts for the decrease of the long spacing (around 2−3 nm) observed at the beginning of the crystallization. A few authors have suggested the opposite hypothesis, i.e., that the large length corresponds to the thickness of the amorphous regions L_a.[16,20−22,35] In this case, a model with a single population of lamellae with a distribution of thicknesses suffices to account for the experimental observations.

The study of the morphology of narrow molecular weight fractions generally greatly helps the understanding of the complex behavior of the polymer with a large degree of polydispersity. Only a limited effort has been devoted to the study of narrow molecular weight fractions and oligomers of PEEK.[36−39] In a previous study, we have investigated the morphology of narrow molecular weight fractions of PEEK ranging from 4000 to 79 000 isothermally crystallized from the glass at various temperatures between 250 and 340 °C.[35] These samples were prepared by heating through the glass transition followed by isothermal annealing for 1 h. They were investigated by X-ray diffraction and DSC after their cooling at room temperature. This paper deals with a time-resolved SAXS, WAXD, and DSC study of the heating of amorphous samples of these PEEK fractions and an industrial grade of PEEK (Stabar K200) from below their glass transition temperature through their melting. The aim is to investigate the morphological modifications occurring during cold crystallization and subsequent melting.

Each sample was heated from below its glass transition temperature (T_g) to 375 °C. A single heating experiment thus includes cold crystallization, reorganization if any, and the final melting of the resulting crystals. The evolution of the lamellar morphology during the entire heating ramp was monitored by time-resolved simultaneous small-angle X-ray scattering (SAXS) and wide-angle X-ray diffraction (WAXD) while the thermal behavior was followed by differential scanning calorimetry (DSC).

Experimental Section

The monodisperse PEEK samples used are the same as those used in a previous study.[35] Their synthesis and some kinetics characteristics are described elsewhere.[37−39] The molecular weights of the PEEK samples used in this work are given in Table 1. Throughout the present paper, the weight-average molecular weight $\bar{M}_w$ (e.g., 18K for a sample with $\bar{M}_w$ = 18 000) is used to characterize the materials. Amorphous films of these fractions were obtained by melting the powders in a laboratory press (Carver) heated at 400 °C for 1 min

[†] Université de Mons-Hainaut.
[‡] European Molecular Biology Laboratory.
[§] National Research Council of Canada.
* Corresponding author.

10.1021/ma9909206 CCC: $18.00
Published on Web 11/10/1999

Table 1. Main Characteristics of the Different PEEK Samples: Number-Average Molecular Weight ($\bar{M}_n$), Weight-Average Molecular Weight ($\bar{M}_w$), Glass Transition Temperature (T_g), Cold Crystallization Temperature (T_{cc}), the Width of the Cold Crystallization Exotherm Measured at Half-Height, the Temperature Where the Overall Crystallization Rate Is Equal to the Overall Melting Rate (T^*), and the Temperature of the Maximum of the Melting Endotherm (T_m)

sample	$\bar{M}_n$	$\bar{M}_w$	T_g (°C)	T_{cc} (°C)	width (°C)	T^* (°C)	T_m (°C)	ΔH_m (J/g)
4K	3 500[b]	4 400[b]	122.5	152.5	3.7	315	344.0	65.0
8K	7 000[b]	8 300[b]	133.5	165.5	3.9	324	350.5	63.6
18K	14 500[b]	18 000[b]	140.0	176.0	4.9	307	349.0	45.6
32K	21 500[b]	32 000[b]	145.5	183.5	5.3	288	339.0	37.3
79K	60 200[b]	79 500[b]	147.5	190.5	9.5	273	325.0	23.5
Stabar K200	35 000−50 000[a]	95 000−120 000[a]	143.0	175.0	3.0	300	339.8	35.6

[a] From ref 49. [b] From ref 39.

followed by rapid quenching in an ice−water mixture. These films were found to be amorphous as checked by wide-angle X-ray diffraction. The commercial grade of PEEK Stabar K200 used in this study was supplied by ICI in the form of amorphous 0.250 mm thick films.

The DSC measurements were made at a scanning rate of 10 °C/min between 100 and 375 °C in a heat flux differential scanning calorimeter (TA Instruments, model 2920) working under nitrogen atmosphere using about 2 mg of each sample. Temperature and heat flow calibrations were made using caffeine, indium, and zinc. A new baseline recorded by running two empty pans was subtracted to the raw heat flow. The glass temperature, the temperature, and heat of melting are given in Table 1. The precision on the values of temperature and heat of melting are 0.5 °C and 1 J/g, respectively.

The WAXD and SAXS curves were recorded simultaneously using two linear position detectors connected in series[40] on the X33 beam line of the EMBL in HASYLAB on the storage ring DORIS III of the Deutsches Elektronen Synchrotron (DESY) at Hamburg.[41,42] Recording times of 20 s were used to obtain high-quality SAXS and WAXS profiles. The SAXS and WAXS intensities were recorded in the range $0.014\ nm^{-1} < s < 0.33\ nm^{-1}$ and $1.3\ nm^{-1} < s < 4\ nm^{-1}$, respectively ($s = 2 \sin \theta/\lambda$ where 2θ is the scattering angle and λ the wavelength of the incident X-ray beam (0.15 nm)). Calibration of the SAXS and WAXD regions was made using collagen and powders of organic compounds (benzoic acid, biphenyl, naphthalene), respectively. Amorphous PEEK films wrapped in thin aluminum foils were heated in a hot stage (Mettler FP82HT) and submitted to the same thermal treatment as in the differential scanning calorimeter. The experimental X-ray intensity curves were corrected for absorption and normalized to the intensity of the primary beam monitored with an ionization chamber, and a background was subtracted. The normalized intensities were Lorentz corrected by multiplying the SAXS data by s^2 and the WAXD intensities data by $\sin 2\theta \sin\theta$ (where s is the scattering vector and 2θ the Bragg angle). To evaluate the correlation function $\gamma(r)$, the fluidlike contribution was estimated from an Is^4 versus s^4 plot and subtracted before extrapolating the SAXS intensity curves to large s values using Porod's law.[43] The lamellar thickness L_c and the amorphous thickness L_a, the long period $L_p^{corr} = L_a + L_c$, and the linear degree of crystallinity v_c^{lin} ($v_c^{lin} = L_c/(L_c + L_a)$) were evaluated according to standard procedures.[44]

The spacings corresponding to the (110), (111), (200), and (211) reflections were evaluated from the positions of the corresponding maxima in the diffraction patterns. The amorphous and crystalline contributions in the WAXD diffraction patterns were separated by fitting an amorphous halo after subtracting a linear background between $1.37\ nm^{-1} < s < 3.5\ nm^{-1}$. Such a procedure allows the determination of the degree of crystallinity of the various samples.

Results

Figure 1a−d illustrates the evolution of the WAXD and SAXS diffraction patterns during the heating at 10 °C/min of low (8K) and high (79K) molecular weight fractions of PEEK. The temperature range where a crystalline phase exists in the sample is broader for the fractions of low molecular weight as expected from the DSC curves (Figure 2). At a given temperature in this range, the long spacing increases with the average molecular weight

Evolution of the Integrated Intensities. Figure 2a−f illustrates the evolution of the SAXS and WAXD intensities (I^{SAXS} and I^{WAXD}) during the heating of each amorphous sample together with the corresponding DSC trace recorded at the same heating rate. In each case, the cold crystallization exotherm seen in the DSC curve is accompanied by a sudden increase of both SAXS and WAXD diffracted intensities. With the resolution time of our experiments, i.e., 20 s per frame, both WAXD and SAXS patterns appear simultaneously. Between the cold crystallization and the melting region, I^{WAXD} is nearly constant or slightly increases to reach its maximum value just before the melting zone. In contrast, a large increase of I^{SAXS} is observed in the same temperature region. This is mainly due to the fact that I^{SAXS} is proportional to the square of the difference between the electron densities of the amorphous and crystalline regions which increases significantly due to differential thermal expansion. In the melting region, the weight degree of crystallinity I^{WAXD} decreases more rapidly on heating than I^{SAXS} as a consequence of thermal disorder. Note also that I^{SAXS} is proportional to $v_c^{lin}(1 - v_c^{lin})$ which decreases more slowly than v_c^{lin}.

Morphology during Nonisothermal Cold Crystallization. The temperature limits of this region can be defined by the points where the DSC signal significantly deviates from the baseline. The width of the cold crystallization exotherm strongly increases with the average molecular weight while its area decreases by a factor of 2 when going from the smallest to the largest average molecular weight (Figure 2 and Table 1). Large modifications of the morphology of the PEEK fractions are therefore expected during the cold crystallization.

Though the data obtained from the correlation functions corresponding to the early stage of the cold crystallization are not taken into account here because of the relatively low scattered intensity of the corresponding diffraction patterns, a clear decrease of the long period L_p^{corr} is observed until the temperature reaches some 20 °C above the cold crystallization temperature (Figure 2). This phenomenon, which has already been reported for nonisothermal crystallization from the glassy state[20] and for isothermal crystallization from the melt,[17,45] is observed for the polydisperse sample (Stabar) as well as for the narrow molecular weight fractions. A molecular weight segregation during crystallization can be ruled out taking into account the low degrees of polydispersity of the PEEK fractions. A marked decrease of the long period is associated with a decrease of the largest length computed from the correlation function, assigned to the amorphous thickness in accordance with our previous works (Figure 3).[21,22,35] At the same time, the thickness of the crystal-

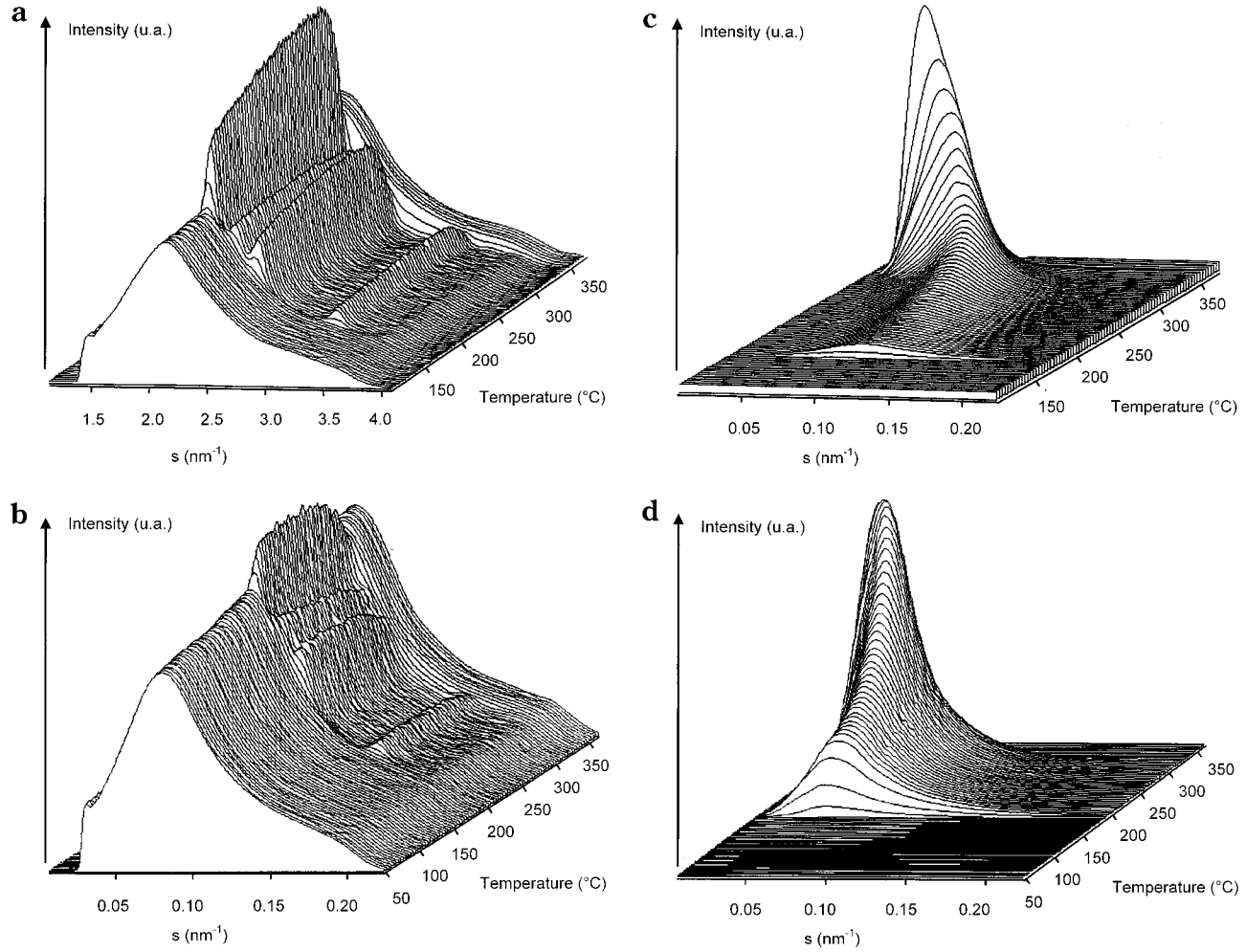

Figure 1. Wide-angle X-ray diffraction patterns recorded during heating of the amorphous 8K (a) and 79K (b) PEEK fractions. Small-angle X-ray scattering patterns recorded during heating of the amorphous 8K (c) and 79K (d) PEEK fractions.

line regions (L_c) only slightly increases or remains constant. This results in an increase of the linear crystallinity v_c^{lin} (Figure 4), which is consistent with the evolution of the degree of crystallinity estimated by DSC.

Morphology between the Cold Crystallization and the Melting Region. The upper temperature of this region (T^* in Figure 2a) is determined by the intersection of the DSC heat flow signal with the baseline drawn from just above the glass transition to the plateau above the final melting point. Below T^*, the overall recrystallization process dominates the overall melting. Between the cold crystallization temperature T_{cc} and T^*, both L_a and L_c slightly increase, leading to an almost constant value of the linear crystallinity v_c^{lin} (Figure 4). The widths of the major WAXD reflections decrease, however, continuously in this temperature range as illustrated for the (110) reflection (Figure 5). This corresponds to an increase of the crystal dimension along the normal to the (110) crystallographic plane.[46] As the other WAXD reflections behave similarly, it can be concluded that the crystals become more perfect during heating. Note that the observed decrease of the width of the reflections should be more larger than estimated since the thermal motions, which always broaden the reflections with increasing temperature, were not taken into account. Figure 5 illustrates that, at the same temperature, the degree of perfection is higher for the lower molecular weight fractions.

Morphology in the Melting Region. This temperature region is characterized by a large increase of the long period mainly due to an increase of the amorphous thickness. Although a pronounced increase of L_c is also observed especially for the low molecular weight fraction, v_c^{lin} decreases abruptly in this temperature range, which is consistent with the decrease of the macroscopic crystallinity. During the first stage of the melting, i.e., below the maximum in the DSC trace, the width of the (110) reflection still decreases for all the samples while in the final melting stage it increases for the higher molecular weight fractions (Figure 5).

Discussion

Morphology. For crystallization from the glass, which is governed by chain mobility rather than by nucleation, the diffusion rate of the very entangled longer chains is much smaller than for the low molecular weight chains leading to a reduced crystallization rate. This finally results in a broadening of the crystallization exotherm. Note that the commercial PEEK (Stabar) has the narrowest exotherm probably due to its high polydispersity. As a part of the chains does not disentangle, the number of entanglements trapped in the amorphous zones increases with the molecular weight. This reduces the amount material that is able to crystallize and thus leads to a decrease of the magnitude of the exotherm. The mode of crystallization used here includes a rapid nucleation process resulting in very small spherulites which impinge very quickly.

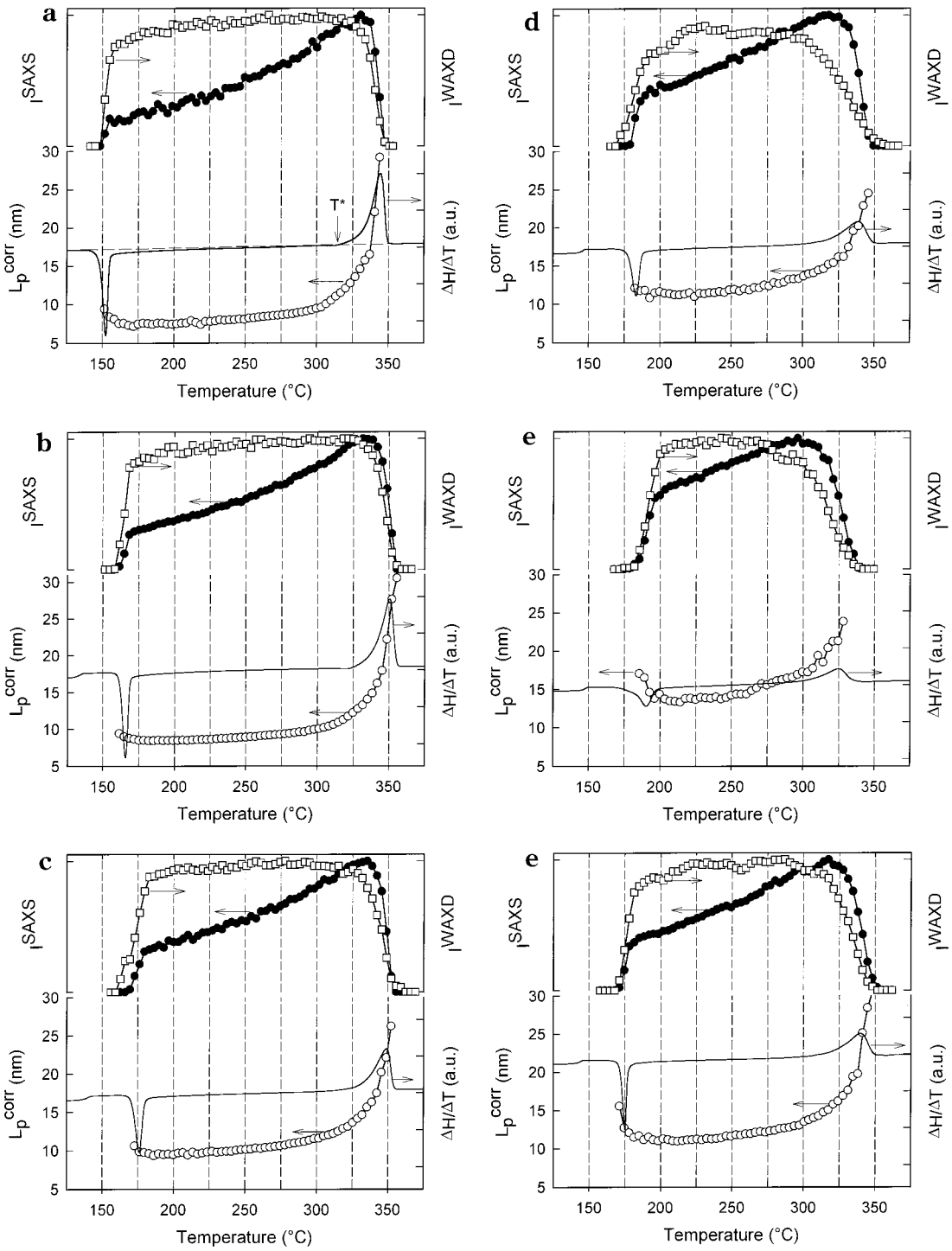

Figure 2. DSC traces, long period obtained from the correlation function, WAXD integrated intensity, and SAXS integrated intensity recorded during heating of initially amorphous samples 4K (a), 8K (b), 18K (c), 32K (d), 79K (e), and PEEK Stabar (f). The same scale is used through all figures.

It is likely that, after the rapid impingement of the spherulites, crystallization would continue within the spherulite main structure. It is observed that the decrease of the long period starts in the narrow crystallization exotherm region and spreads out to somewhat higher temperatures (Figures 2). This observed decrease of the long period occurs simultaneously with a progressive filling with crystals of the amorphous gaps left between the first grown lamellae. Because of an averaging effect, the amorphous thickness L_a and the long spacing L_p decrease with time. There is no significant decrease of L_c during this step, which indicates that the crystals grown at the beginning and at the end of the cold crystallization region have a similar thickness (Figure 3). At the end of the cold crystallization, a single population of crystalline lamellae with a given thickness distribution can be considered as representative for the morphology of the PEEK fractions. The thermal evolution of the crystalline length L_c superimposes for all the fractions whereas the amorphous length L_a increases with increasing molecular weight (Figure 3). Our assignment of L_a and L_c which implies that, at a given temperature, L_c is almost independent of the molecular weight while L_a strongly increases, is in agreement with

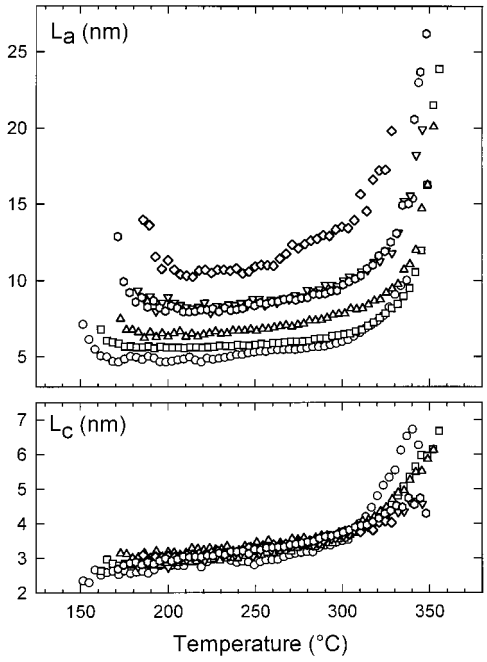

Figure 3. Crystalline (L_c) and amorphous (L_a) thicknesses obtained from the correlation function during heating of the various samples 4K (○), 8K (□), 18K (△), 32K (▽), 79K (◇), and Stabar (⬡).

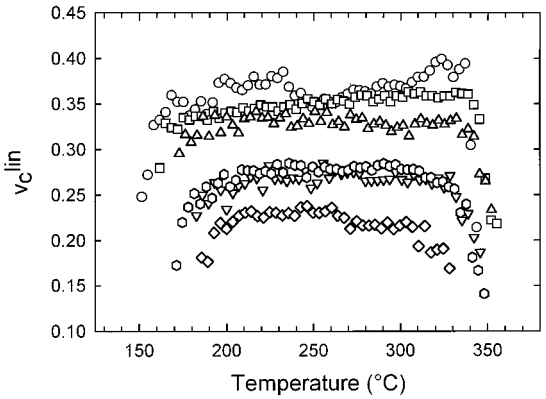

Figure 4. Linear degree of crystallinity v_c^{lin} during heating of various PEEK samples 4K (○), 8K (□), 18K (△), 32K (▽), 79K (◇), and Stabar (⬡).

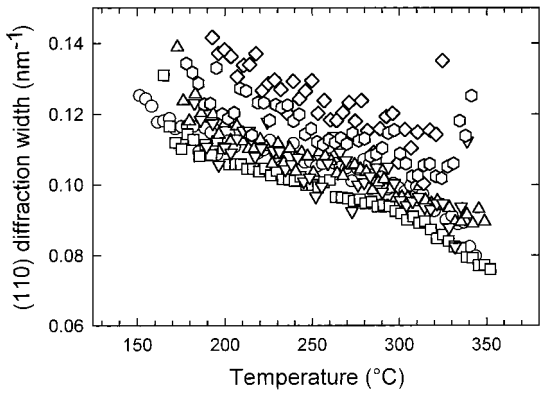

Figure 5. Thermal evolution of the full width at half-maximum of the (110) reflection for PEEK samples 4K (○), 8K (□), 18K (△), 32K (▽), 79K (◇), and Stabar (⬡).

our previous observations on the same PEEK fractions crystallized and annealed from the glassy state[35] and is also documented for other semicrystalline polymers.[47,48] At the same degree of supercooling, the crystal thickness L_c should be nearly independent of the molecular weight. In contrast, the thickness of the amorphous regions separating stacked lamellae is expected to increase with the molecular weight due to entanglements.[47] Although the present results are obtained in nonisothermal conditions, they are in agreement with scaling law predictions and confirm the assignment of the smallest length computed from the correlation function to the crystalline thickness L_c and thus $L_a > L_c$. Great difficulties are encountered when trying to justify our experimental results with the reverse picture (i.e., $L_a > L_c$). Small increases of the equilibrium melting temperature T_m^0 with increasing average molecular weight have been suggested for these PEEK fractions[38] and would result, for the same crystallization temperature, in larger degrees of supercooling for increasing molecular weights. According to Tamman's equation, this would lead to an decrease of L_c with increasing average molecular weight which cannot be reconciled with the hypothesis that $L_c > L_a$. Therefore, it can be concluded that the linear crystallinity decreases with increasing molecular weight at a given temperature (Figure 4). This proposal is also consistent with the DSC results showing that the total exotherm contribution is more important for the low molecular weight fractions.

Reorganization of the Initial Morphology. Between cold crystallization temperature T_{cc} and $T_{cc} + 100$ °C, the average thermal dependence of the crystal thickness L_c for the different samples can be reasonably fitted to following equation

$$L_c = (18 \pm 4)[1 + (0.0028 \pm 0.0009)T]$$

where T is the temperature in °C. The value of 2.8×10^{-3} °C^{-1} has to be compared with the thermal expansion coefficient which is on the order of 2×10^{-5} °C^{-1} in the direction perpendicular to the basal plane of the lamellae (i.e., along the *c* crystallographic axis).[20] The increase of L_c reported here is by far too large to be due to thermal expansion only. The morphology resulting from the cold crystallization is therefore unstable and will thus reorganize to some extent. The imperfect crystals grown at T_{cc} recrystallize upon subsequent heating. Further evidence in favor of this proposal comes from the analysis of the width of the reflections which indicates a continuously increasing crystal perfection with increasing temperature from T_{cc} to the final melting. The lamellae thus reorganize during the entire temperature scan. It can be assumed that the reorganization process leads to thickening of the lamellae in the chain axis direction and/or an increase of the lateral dimensions of the crystals (i.e., a lower mosaicity of the lamellar assembly). The crystalline thickness of all fractions follows the same thermal evolution at least between T_{cc} and T^*: the crystals made during the cold crystallization thicken in about the same fashion whatever the value of the average molecular weight (Figure 3). In contrast, analysis of the width of the reflections shows that the lateral dimensions of the crystals significantly decrease with increasing molecular weight at a given temperature. It can be assumed that during crystallization the number of chains that cannot disentangle, because they do not end in the amorphous zone, is statistically much larger for the high molecular weight samples. It should be remembered that the extended chain of the smallest fraction (4K) is 20 times shorter than that of the highest molecular weight fraction (79K). A straightforward consequence of this

is that the amorphous thickness L_a increases with molecular weight. Moreover, as high molecular weight chains are less able to relax in amorphous regions, the stress created at the crystal−amorphous interface during crystallization is higher for the high molecular weight fractions. This last phenomenon impedes the lateral reorganization of the lamellae for the longest chains. At the end of the melting, the value of L_c obtained for the shorter fraction (4K, 8K, 18K) are found to increase to some 6−7 nm. We believe that chain mobility accounts for this observation: as the number of entanglements is relatively lower for these short fractions, reorganization is much easier than for the entangled high molecular weight fractions. At high degrees of supercooling, just above the cold crystallization where the crystallization rate is relatively important, this does not make a marked difference between the various samples. In contrast, at low degrees of supercooling, short chains reorganize easily into more stable crystals whereas long chains are unable to do so in the same scale time. This also accounts for the broadening of the DSC melting endotherm for the high molecular weight fractions: as long as reorganization is possible, the crystals melt immediately, and this is followed by recrystallization. The DSC signal, being the sum of both exothermic and endothermic contributions, remains close to the baseline. This is the case for 4K and 8K fractions up to relatively high temperatures where the overall recrystallization rate becomes very small, while the DSC signal recorded during the heating of the 79K for example starts to deviate from the baseline at much lower temperature.

Conclusion

The thermal evolution of the morphology of nonisothermally cold crystallized narrow molecular weight fractions of PEEK has been interpreted by considering a single population of lamellar crystals with an usual thickness distribution. The lamellae grow in the cold crystallization region and perfect during the heating process. The decrease of the long period observed in the early stage of crystallization results from a densification of the interlamellar amorphous regions due to a more easy rearrangement of the chains in such low-density regions. The crystalline thickness is nearly constant during the first stage of crystallization. Upon heating, both the crystalline and amorphous layers thicken. However, the thermal evolution of the crystalline thickness L_c is independent of the average molecular weight whereas the thickness of the amorphous regions strongly increases. This was attributed to differences in the interlamellar amorphous material, i.e., differences in the degree of entanglement of the various samples. This phenomenon also accounts for the fact that the lowest crystal perfection corresponds to the highest molecular weight fractions. The behavior of the commercial Stabar is similar to that of the 32K fraction except in the cold crystallization region where the former crystallizes faster, probably due to its larger degree of polydispersity.

Acknowledgment. This work was supported by the Belgian National Funds for Scientific Research and the European Union through the HCMP Access to Large Installations Project, Contract CHGE-CT93-0040, to the EMBL.

References and Notes

(1) Blundell, D. J.; Osborn, B. N. *Polymer* **1983**, *24*, 953.
(2) Velisaris, C.; Seferis, J. *Polym. Eng. Sci.* **1986**, *26* (22), 1574.
(3) Nguyen, H. X.; Ishida, H. *Polym. Compos.* **1987**, *8*, 57.
(4) Blundell, D. J.; Osborn, B. N. *Polymer* **1983**, *24*, 953.
(5) Cheng, S. Z. D.; Cao, M.-Y.; Wunderlich, B. *Macromolecules* **1986**, *19*, 1868.
(6) Blundell, D. J. *Polymer* **1987**, *28*, 2248.
(7) Cebe, P.; Chung, S.; Hong, S. D. *J. Appl. Polym. Sci.* **1987**, *33*, 487.
(8) Lee, Y.; Porter, R. S. *Macromolecules* **1987**, *20*, 1336.
(9) Cebe, P. *J. Mater. Sci.* **1988** , *23*, 3721.
(10) Lee, Y.; Porter, R. S.; Lin, J. S. *Macromolecules* **1989**, *22*, 1756.
(11) Rueda, D. R.; Ania, F.; Richardson, A.; Ward, I. M.; Balta Calleja, F. J. *Polym. Commun.* **1983**, *24*, 258.
(12) Wakelyn, N. T. *J. Polym. Sci., Polym. Lett.* **1987**, *25*, 25.
(13) Hay, J. N.; Langford, J. I.; Lloyd, J. R. *Polymer* **1989**, *30*, 489.
(14) Zimmermann, H. J.; Konnecke, K. *Polymer* **1991**, *32*, 3162.
(15) Iannelli, P. *Macromolecules* **1993**, *26*, 239.
(16) Wang, J.; Alvarez, M.; Zhang, W.; Wu, Z.; Li, Y.; Chu, B. *Macromolecules* **1992**, *25*, 6943.
(17) Hsiao, B. S.; Gardner, K. H.; Wu, D. Q.; Chu, B. *Polymer* **1993**, *34*, 3986.
(18) Hsiao, B. S.; Gardner, K. H.; Wu, D. Q. *Polymer* **1993**, *34*, 3996.
(19) Krüger, K.-N.; Zachmann, H. G. *Macromolecules* **1993**, *26*, 5202.
(20) Jonas, A. M.; Russell, T. P.; Yoon, Do, Y. *Macromolecules* **1996**, *28*, 8491.
(21) Fougnies, C.; Damman, P.; Villers, D.; Dosière, M.; Koch, M. *Macromolecules* **1997**, *30*, 1385.
(22) Fougnies, C.; Damman, P.; Dosière, M.; Koch, M. H. J. *Macromolecules* **1997**, *30*, 1392.
(23) Verma, R.; Marand, H.; Hsiao, B. *Macromolecules* **1996**, *29*, 7767.
(24) Wang, W.; Schultz, J. M.; Hsiao, B. *J. Macromol. Sci., Phys.* **1998**, *B37*, 667.
(25) Bassett, D. C.; Olley, R. J.; Al Raheil, I. A. M. *Polymer* **1988**, *29*, 1745.
(26) Lovinger, A. J.; Davis, D. D. *Polym. Commun.* **1985**, *26*, 322.
(27) Lovinger, A. J.; Davis, D. D. *J. Appl. Phys.* **1985**, *58*, 2843.
(28) Lovinger, A. J.; Davis, D. D. *Macromolecules* **1986**, *19*, 1861.
(29) Olley, R. H.; Bassett, D. C.; Blundell, D. J. *Polymer* **1986**, *26*, 344.
(30) Chung, C. T.; Chen, M. *Polym. Prepr., ACS San Francisco Meeting* **1992**, *33*, 420.
(31) Zhang, Z.; Zeng, H. *Makromol. Chem.* **1992**, *193*, 1745.
(32) Zhang, Z.; Zeng, H. *Polymer* **1993**, *34*, 1551.
(33) Zhang, Z.; Zeng, H. *Polymer* **1993**, *34*, 4032.
(34) Verma, K. R.; Hsiao, B. S. *Trends Polym. Sci.* **1996**, *4*, 312.
(35) Fougnies, C.; Dosière, M.; Koch, M. H. J.; Roovers, J. *Macromolecules* **1998**, *31*, 6266.
(36) Jonas, A.; Legras, R.; Scerrenberg, R.; Reynaers, H. *Macromolecules* **1993**, *26*, 526.
(37) Day, M.; Deslandes, Y.; Roovers, J.; Suprunchuk, T. *Polymer* **1991**, *32*, 1258.
(38) Deslandes, Y.; Sabir, F.-N.; Roovers, J. *Polymer* **1991**, *32*, 1267.
(39) Roovers, J.; Cooney, J. D.; Toporowski, P. M. *Macromolecules* **1990**, *23*, 1611.
(40) Rapp, G.; Gabriel, A.; Dosière, M.; Koch, M. H. J. *Nucl. Instrum. Methods* **1995**, *A357*, 178.
(41) Koch, M. H. J.; Bordas, J. *Nucl. Instrum. Methods* **1983**, *A208*, 461.
(42) Boulin, C. F.; Kempf, R.; Gabriel, A.; Koch, M. H. J. *Nucl. Instrum. Methods* **1988**, *A269*, 312.
(43) Balta-Calleja, F. J.; Vonk, C. G. In *X-ray Scattering of Synthetic Polymers*; Elsevier: Amsterdam, 1989; Chapter 7.
(44) Strobl, G. R.; Schneider, M. J. *J. Polym. Sci., Polym. Phys. Ed.* **1980**, *18*, 1343.
(45) Hsiao, S. B.; Sauer, B. S.; Verma, R. K.; Zachmann, H. G.; Seifert, S.; Chu, B.; Harney, P. *Macromolecules* **1995**, *28*, 6931.
(46) Alexander, L. E. *X-ray Diffraction Methods in Polymer Science*; John Wiley and Sons: New York, 1954.
(47) Rault, J.; Robelin-Souffaché, E. *J. Polym. Sci., Polym. Phys. Ed.* **1989,** *27*, 1349.
(48) Mandelkern, L.; Alamo, R. G.; Kennedy, M. A. *Macromolecules* **1990**, *23*, 4721.
(49) Bas, C.; Cooney, J. D.; Albérola, N. D. *J. Appl. Polym. Sci.* **1994**, *53*, 1745.

MA9909206